Lab on a Chip

Accepted Manuscript

ROYAL SOCIETY OF CHEMISTRY

www.rsc.org/loc

Journal Name

RSCPublishing

TECHNICAL INNOVATION

Cite this: DOI: 10.1039/x0xx00000x

A superhydrophobic chip based on SU-8 photoresist pillars suspended on a silicon nitride membrane†

Received ooth January 2012,
Accepted ooth January 2012

DOI: 10.1039/x0xx00000x

www.rsc.org/

Giovanni Marinaro[a,b], Angelo Accardo[b], Francesco De Angelis[b], Thomas Dane[a], Britta Weinhausen[a], Manfred Burghammer[a,c] and Christian Riekel[a]

We developed a new generation of superhydrophobic chips optimized for probing ultrasmall sample quantities by X-ray scattering and fluorescence techniques. The chips are based on thin Si_3N_4 membranes with a tailored pattern of SU-8 photoresist pillars. Indeed, aqueous solution droplets can be evaporated and concentrated at predefined positions by a non-periodic pillar pattern. We demonstrate quantitatively the deposition and aggregation of gold glyconanoparticles from the evaporation of a nanomolar droplet in a small spot by raster X-ray nanofluorescence. Further, raster nanocrystallography on biological objects such as rod-like tobacco mosaic virus nanoparticles reveals crystalline macro-domain formation composed of highly oriented nanorods.

Introduction

The sensitivity for probing low molecular concentrations of molecules or nanoparticles by X-ray scattering techniques can be considerably amplified by evaporating quasi contact-free droplets on superhydrophobic surfaces (SHSs).[1] Indeed, assembly processes at the interface of an evaporating droplet or the heterogeneity of its residue can be probed in-situ by raster-scan X-ray diffraction (XRD) with µm- or sub-µm step-resolution defined by the focal spot size.[1] The absorption of SHSs based on standard silicon wafers of ~500 µm thickness is, however, ~82 % at λ=0.1 nm wavelength.[2] This poses no problem if the X-ray beam is oriented parallel to the surface when probing a droplet.[1] Raster-scan probing of residues in transmission geometry can also often be performed after separating the residue from the substrate.[3] This is not possible for fragile residues such as filamentous extensions. Such morphologies are, however, of particular interest for XRD probing due to extensional flow alignment during the pinning transition.[1] An alternative is using SHSs based on thin Si-substrates with holes etched between the pillars.[4] Although the X-ray absorption of a ~50 µm thick Si-substrate is only ~16 %, the correction for variation in absorption due to the presence of holes requires elaborate post-processing software. Our aim was therefore developing a SHS showing a high, quasi-homogeneous X-ray transmission and incorporating a periodic as well as non-periodic pillar patterning.[5, 6] This latter feature can help keeping the droplet localized during evaporation or predefine the position of a residue-speckle for probing by an X-ray beam.[6]

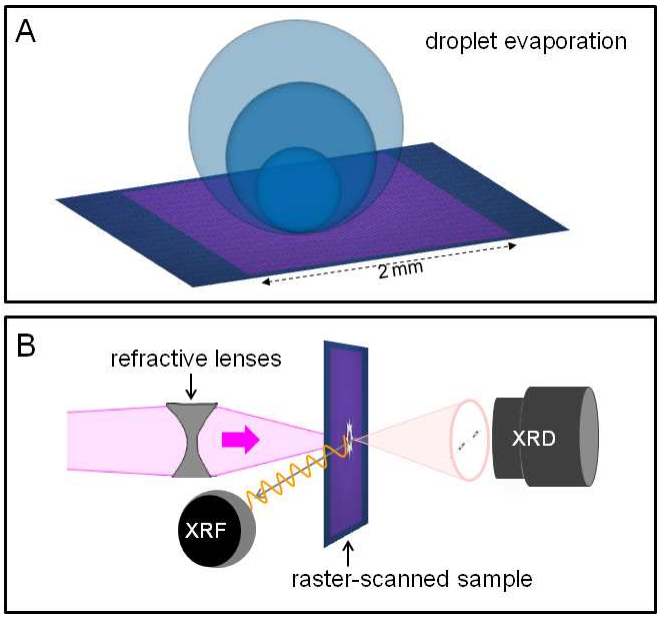

Fig.1 **A**: An about 4 µL droplet is evaporated on the Si_3N_4 membrane equipped with superhydrophobic SU8 micropillars and the solute is concentrated. **B**: Schematic experimental setup allowing XRD and XRF experiments. The monochromatic beam from an undulator source is focused by refractive lenses[7] to a submicron spot on the sample. The residue is raster-scanned through the nanobeam. An XRD pattern and XRF spectrum (optionally) are recorded at every position.

We report here on the fabrication of SHS-chips based on a 0.5 µm thick Si_3N_4 substrate (~99.9% X-ray transmission) and ~12 µm high SU-8 photoresist pillars (~99.8 % X-ray transmission) showing also high optical and IR transmissions. To explore the solution concentration capability of the chips we probed a gold

glyconanoparticle residue by nanobeam X-ray fluorescence (nanoXRF). As an example for a weakly scattering biomaterial we studied a tobacco mosaic virus (TMV) residue by nanobeam X-ray diffraction (nanoXRD). The experimental protocol and setup are shown schematically in **Figs.1A,B.**

Materials and Methods

Device microfabrication

We fabricated three masks for generating (i) a matrix of Si_3N_4 membranes, (ii) a periodic, hexagonal lattice of 10 μm diameter SU-8 pillars with a 30 μm pitch[8] and (iii) a non-periodic lattice of SU-8 pillars defined by an analytical function with the pillar-separation decreasing towards the center of the chip thus inducing a gradient in wettability.[5, 6] We used a 2 inch <100> orientation silicon wafer with a 0.5 μm Si_3N_4 layer on both sides. A photolithography step was used to protect the membrane from the following reactive ion etch (RIE) process uncovering the silicon according to the pattern of the 1st mask defining the Si-frames of the membranes of the individual chips. The silicon was removed by wet etching with KOH solution. A layer of SU-8 photoresist was then spin-coated on the wafer and structured by a 2nd photolithography process on the other side of the chip which involved an alignment step to match the pattern of the frames on the opposite side. The pillars and Si_3N_4 membrane were covered with a ~20 nm thick Teflon (C_4F_8) layer by plasma deposition. (Supplementary Information)

The SHS-chips were characterized by optical microscopy and scanning electron microscopy (SEM) (**Figs.2A,B;3A,B**). We measured a contact angle for a 4 μL water droplet of Θ=151.2° on a periodic pillar SHS-chip. (Supplementary Information)

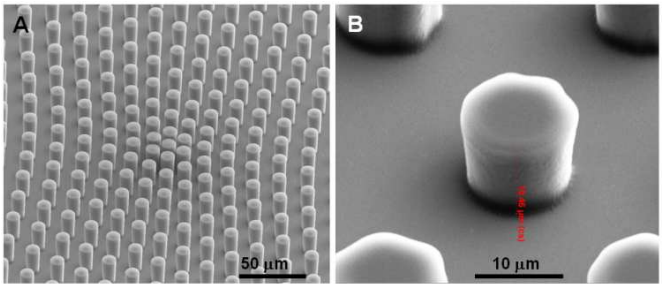

Fig.2 A: Scanning electron microscopy (SEM) image of central part of non-periodic SU-8 pillar lattice on Si_3N_4 substrate. **B**: Single SU-8 pillar of ~10 μm height. The pillars and substrate are covered by a ~20 nm layer of Teflon

Materials

Colloidal gold nanoparticles (AuNPs) with ligand-functionalized surfaces provide elements for bottom-up assembly of functional nanostructures which are of interest for mimicking biological systems.[9] We deposited a ~4 μL droplet of 5 nM gold glyconanoparticles in deionized water on the SHS-chip. (**Fig.1A**) The ~2.9 nm diameter particles consist of a 1.3 ±0.3 nm diameter core corresponding on average to 71 gold atoms and were functionalized with a ~0.8 nm carbohydrate shell.[10] We will use below the abbreviation Au_{71}NP. (Supplementary Information)

TMV is a plant-virus forming filamentous structures.[11] The TMV particles have a rod-like shape of ~300 nm length and ~18 nm diameter.[12] We used a solution with 405 mg/ml TMV particles in 1 mM EDTA solution + 0.1% azide, pH 7.2. The solution was diluted by factor 100 by deionized water. The deposited droplet volume was set as well to ~4 μL.

The SU-8 25 photoresist was obtained from MicroChem.

Synchrotron radiation experiments

A λ=0.08321 nm monochromatic X-ray beam was focused to a ~170(h)x130(v) nm^2 spot by Si refractive lenses[7] with a flux of ~$2x10^9$ photons/s at the sample position. Experiments were performed in transmission geometry with the beam normal to the substrate. (**Fig.1B**) XRF spectra were recorded in the horizontal scattering plane by a Si-drift detector. XRD data were collected by a CCD camera with X-ray converter screen and 2Kx2K pixels of 50x50 μm^2 each. The sample was step-scanned through the beam using an x/y/z piezo-stage. (Supplementary Information) Background scattering from the substrate was very small and did not contribute discrete peaks or short-range order to the XRD patterns.

Results and discussion

NanoXRF probing of gold nanoparticles

Optical and SEM images of the Au_{71}NP residue on the non-periodic SHS-chip are shown in **Figs.3A,B.** The composite XRF image (C-XRF) is composed of "pixels" scaled to the local integrated Au L_α band. (**Fig.3C**) The azimuthally integrated XRF profile is shown in **Fig.3D**. Two Gaussian profiles were fitted to the XRF profile suggesting two deposition zones around the chip-center. (**Fig.3D**) Residue deposited close to the center of the gradient pattern extends radially to ~50 μm. This is surrounded by a broader residue distribution extending radially to ~150 μm. We attribute this to nanoparticles deposited at the contact-line during the pinning-transition. Although a number of pillars are connected by filaments (**Fig.3B**), the nanoparticle concentration was not high enough for forming a continuous coffee-ring type[13] residue. The XRF profile shows complete confinement of the nanoparticles within the two zones. We note that for ultralow concentrations of organic and biological matter, residue is only deposited in the central zone.[5]

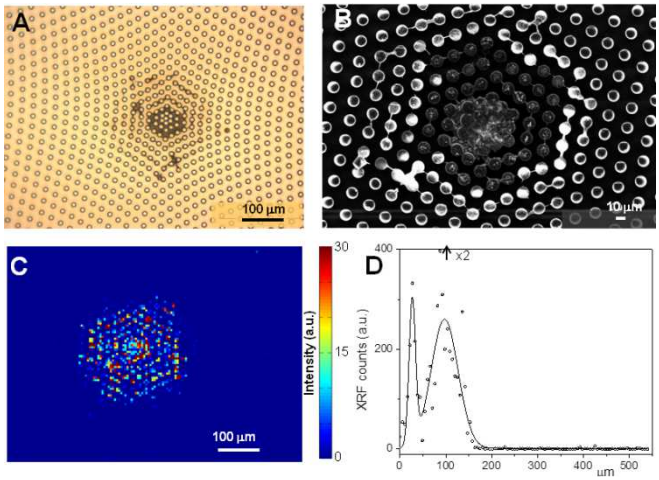

Fig. 3 A: Optical image of gold nanoparticles deposited on a non-periodic pillared SHS-chip. **B**: SEM image of inner part of SHS showing pillars interconnected by filaments. **C**: C-XRF corresponding to a step-resolution of 5 μm based on Au L_α band. **D**: Radial XRF profile obtained by azimuthally integrating the C-XRF. Two Gaussian profiles have been fitted as guides-to-the-eye. The center (0 μm) is defined at the highest pillar density (**Fig.2A**).

Nanodiffraction probing of TMV nanorods

The optical image of a part of the TMV residue deposited on a periodic, pillared SHS-chip shows the formation of a coffee-ring type residue[13] on the pillars. (**Fig.4A**) A composite XRD (C-XRD)

image[14] based on a raster-scan with 0.5 μm steps is shown in **Fig.4B**. Each "pixel" corresponds to a single diffraction pattern as the one shown in **Fig.4C**. The observed reflections agree to the hexagonal TMV lattice with the nanorods oriented along the c-axis.[15] The helical pitch of 2.202 (5) nm derived from the n=3 layer-line reflections confirms the small pitch-reduction for dried TMV residues[15] as compared to TMV sols.[16]

The limitation of the display-range to the strongest, low-order reflections on the n=0 layer-line (**Fig.4C)** implies that Ewald's sphere[17] is large with respect to interatomic distances and the reflection conditions is fulfilled for all patterns. Given a quasi-constant microstructure across the scanned area, the C-XRD image reflects in first order mass density modulations projected on a plane normal to the beam direction.[14]

The C-XRD image reveals increased deposition around the inner-rim pillar as well as for a narrow transition zone between the outer-rim pillar and the outer rim interface. (**Fig.4B**) There is also increased deposition in an area connecting the inner-rim and outer-rim pillars. We even observe in the optical and C-XRD images a thin residue layer on the outer-rim pillar which is the remnant of the retreating triple contact-line. (**Figs.4A,B**)

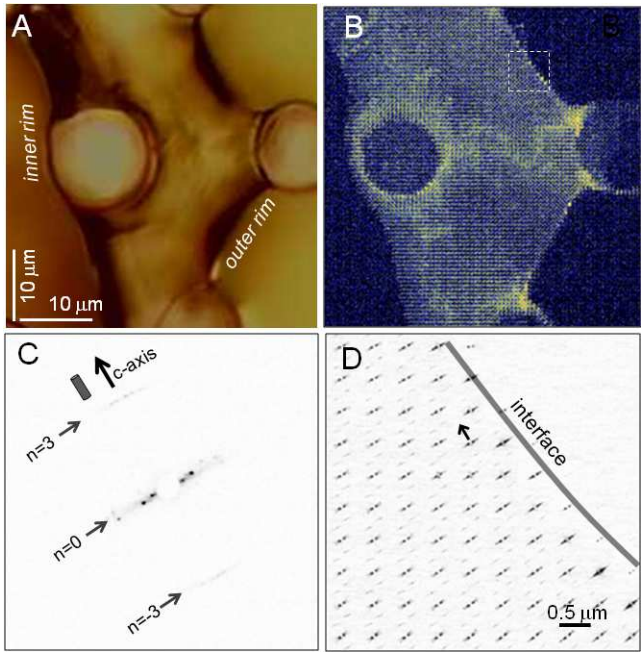

Fig. 4 A: Optical image of TMV residue on periodic pillared SHS-chip. **B**: C-XRD image based on an 81x81 "pixels" mesh scan with 0.5 μm step size. **C**: Single XRD pattern from outer-rim interface. The positions of equator (n=0) and n=3/-3 layer lines are indicated. The c-axis direction (arrow) corresponds also the direction of the long axis of the schematically depicted TMV nanorod.[15] **D**: C-XRD image for dashed square in **(B)** with schematic interface line. The upper display-range is limited to the n=3/-3 layer-lines although scattering from the n=6/-6 layers was also observed. The orientation of the local c-axis, corresponding to the TMV nanorod-axis, is indicated by an arrow.

A more detailed microstructural analysis of the local nanorod orientation provides information on the arrested flow pattern of the nanorods. Indeed, we note the formation of a macrodomain at the outer rim with the nanorod axes aligned parallel to the interface. (**Fig.4D**) Such an orientation has also been observed for the rim of a TMV coffee-ring on a glass substrate and attributed to capillary effects.[15] A more detailed analysis of the arrested nanorods flow pattern is beyond the scope of the present note.

Conclusions

SHS-chips based on a thin Si_3N_4 membrane with periodic and non-periodic SU-8 photoresist pillar patterns have been fabricated and tested by nanobeam XRF and XRD. Well defined compaction of gold nanoparticles was obtained in the center of a non-periodic pillar pattern. The Si_3N_4 membrane and the SU-8 pillars show very high X-ray transmission and low background scattering. Weak diffraction signals from highly oriented TMV nanorods at the residue interface could be observed without background correction. Macrodomain formation by flow-alignment could be explored for other large anisotropic biological objects in order to induce long-range order.

Acknowledgements

We wish to thank F. Gentile (IIT-Genova) and E. Di Fabrizio (KAUST) for very helpful suggestions in the context of the current work. We also thank J.L. Pellequer (CEA Marcoule (IBEB, Service de Biochimie et Toxilogie Nucléaire, Bagnols sur Cèze, France) for a gift of the TMV particle solution and M. Reynolds (ESRF) for the gold nanoparticle solution. I. Snigireva (ESRF Imaging Laboratory) collected the gold nanoparticle residue SEM image. All other SEM images were recorded at IIT-Genova.

Notes and references

[a] European Synchrotron Radiation Facility, B.P.220, F-38043 Grenoble Cedex France,
[b] Istituto Italiano di Tecnologia, Via Morego 30, Genova 16163, Italy
[c] Department of Analytical Chemistry Ghent University Krijgslaan 281, S12B-9000 Ghent, Belgium

Electronic Supplementary Information (ESI) available: [See DOI: 10.1039/b000000x/

1. A. Accardo, E. D. Fabrizio, T. Limongi, G. Marinaro and C. Riekel, *J. Synchr. Rad.*, 2014, **21**, 643-653.
2. B. L. Henke, E. M. Gullikson and J. C. Davis, *Atomic Data and Nuclear Data Tables* 1993, **54**, 181-342.
3. A. Accardo, M. Burghammer, E. D. Cola, M. Reynolds, E. D. Fabrizio and C. Riekel, *Langmuir*, 2011, **27**, 8216-8222.
4. F. Gentile, G. Das, M. L. Coluccio, F. Mecarini, A. Accardo, L. Tirinato, R. Tallerico, G. Cojoc, C. Liberale, F. D. Angelis and E. D. Fabrizio, *Microelectronic Engineering*, 2010, **87**, 798-801
5. F. Gentile, M. L. Coluccio, E. Rondanina, S. Santoriello, D. Di Mascolo, A. Accardo, M. Francardi, F. De Angelis, P. Candeloro and E. Di Fabrizio, *Microelectronic Engineering*, 2013, **111**, 272-276.
6. E. Miele, M. Malerba, M. Dipalo, E. Rondanina, A. Toma and F. D. Angelis, *Adv. Materials*, 2014, **24**, 4179–4183.
7. C. G. Schroer, R. Boye, J. M. Feldkamp, J. Patommel, A. Schropp, A. Schwab, S. Stephan, M. Burghammer, S. Schoder and C. Riekel, *Phys Rev Lett*, 2008, **101**, 090801.
8. F. De Angelis, F. Gentile, F. Mecarini, G. Das, M. Moretti, P. Candeloro, M. L. Coluccio, G. Cojoc, A. Accardo, C. Liberale, R. P. Zaccaria, G. Perozziello, L. Tirinato, A. Toma, G. Cuda, E. Cingolani and E. Di Fabrizio, *Nat Photonics*, 2011, **5**, 683-688.
9. B. Pelaz, S. Jaber, D. J. d. Aberasturi, W. Wulf, T. Aida, J. M. d. l. Fuente, H. E. Gaub, L. Josephson, C. K. Kagam, N. A. Kotov, L. M.

Liz-Marzan, H. Matoussi, P. Mulvaney, C. B. Murray, A. L. Rogach, P. S. Weiss, I. Willner and W. J. Parak, *Acs Nano*, 2012, **6**, 8468-8483.
10. M. Reynolds, M. Marradi, A. Imberty, S. Penades and S. Perez, *Chem. Eur. J.*, 2012, **18**, 4264-4273.
11. A. Kendall, M. McDonald, W. Bian, T. Bowles, S. C. Baumgarten, J. Shi, P. L. Stewart, E. Bullitt, D. Gore, T. Irving, W. M. Havens, S. A. Ghabrial, J. S. Wall and G. Stubbs, *J. Virol.*, 2008, **82**, 9546-9554.
12. A. Klug, *Phil. Trans. R. Soc. Lond. B*, 1999, **354**, 531-535.
13. R. D. Deegan, O. Bakajin, T. F. Dupont, G. Huber, S. R. Nagel and T. A. Witten, *Nature*, 1997, **389**, 827-829.
14. C. Riekel, M. Burghammer, R. Davies, R. Gebhardt and D. Popov, in *Applications of Synchrotron Light to Non-Crystalline Diffraction in Materials and Life Sciences*, eds. M. García-Gutiérrez, A. Nogales, M. Gómez and T. A. Ezquerra, Springer, Heidelberg, 2008.
15. R. Gebhardt, J. M. Teulon, J. L. Pellequer, M. Burghammer, J. P. Colletier and C. Riekel, *Soft Matter*, 2014, **10**, 5458-5462.
16. A. Kendall, M. McDonald and G. Stubbs, *Virology*, 2007, **369**, 226-227.
17. G. Giacovazzo, ed., *Fundamentals of Crystallography*, Oxford University Press, New York, 1992.